Nuclear Spin Pumping Study of Relaxation and Defects in Sodium Bromate*

J. W. DOANE† AND R. A. HULTSCH
Department of Physics, University of Missouri, Columbia, Missouri
(Received 20 October 1965)

The Br^{79} spins in a single crystal of $NaBrO_3$ in a 7086-G magnetic field have a Zeeman-split nuclear-quadrupole-resonance spectrum of four transitions near 180 Mc/sec and one near 10 Mc/sec. The 10-Mc/sec absorption intensity is observed to be enhanced, decreased, or inverted when the crystal is irradiated at one of the four high frequencies. Steady-state nonequilibrium level populations during this nuclear-spin pumping are described by solutions of the rate equations. A value for the ratio of the quadrupolar spin-lattice relaxation probabilities $W_1(\Delta m=\pm 1)/W_2(\Delta m=\pm 2)=5.3\pm 2$ is obtained. Details of the data are interpreted as showing the effects of defective crystalline electric-field-gradient directions θ relative to the magnetic-field direction, as well as defective field-gradient magnitudes. This interpretation is based on differences in $d\nu/d\theta$ of the Zeeman transitions. It appears that only about 50% of the spins contributing to the 10-Mc/sec absorption are reached by the pumping fields.

I. INTRODUCTION

A. Previous Work

THE problem of interest here is understanding nuclear spin-lattice relaxation due to electric quadrupole interactions with a vibrating lattice. That this mechanism is important was shown by Pound[1] in the first demonstration of nuclear spin pumping. One characteristic of quadrupole relaxation is that two transition probabilities per second, W_1 and W_2, associated with $\Delta m=\pm 1$ and $\Delta m=\pm 2$, respectively, are permitted by the quadrupolar Hamiltonian. The magnetic Hamiltonian allows only $\Delta m=\pm 1$ and therefore only one transition probability.

Measurements of spin-lattice relaxation times T_1 of nuclei do not give as detailed information as one would like for understanding relaxation processes. It is known that in ionic crystals at room-temperature quadrupole interactions give T_1's of the order of milliseconds, whereas magnetic interactions alone give times of seconds or minutes. Thus relatively short relaxation times may be ascribed practically entirely to quadrupole effects. However, since T_1 (quadrupolar) $=1/2(W_1+W_2)$ (for spin $\frac{3}{2}$), values of T_1 give no information on the relative magnitudes of W_1 and W_2.

Pound's work showed not only the importance of quadrupolar relaxation, but also a method for measuring the ratio W_1/W_2. His method used simultaneous irradiation at two radio frequencies of the system Na^{23} in a single crystal of $NaNO_3$. Because of small quadrupole shifts of the Zeeman levels, this system gives three closely spaced nuclear-magnetic-resonance absorptions. Pound observed that when one of the transitions was strongly irradiated, another transition showed increased or decreased absorption intensity. These results were interpreted to mean that T_1 of Na^{23} in $NaNO_3$ did not depend solely on magnetic relaxation, but that both W_1 and W_2 quadrupole transition probabilities were important. Using steady-state solutions of the rate equations for the level populations when one transition was saturated, and the observed saturation enhancements, Pound obtained $W_1/W_2\approx 1$.

Weber[2] used pulse techniques to obtain W_1 and W_2 separately for Cl^{35} in $NaClO_3$, $KClO_3$, and paradichlorobenzene. Chlorine spins give a single pure quadrupole transition near 30 Mc/sec in these compounds, and Weber applied a magnetic field of 75 G to split the spectrum into four transitions. His experiment was to pulse one transition and observe the recovery from nonequilibrium of another. Using transient solutions of the rate equations Weber obtained, for example for Cl^{35} in $NaClO_3$, $W_1=8.5\pm 1$ sec^{-1} and $W_2=2.7\pm 1$ sec^{-1}. These values give $W_1/W_2=3.1$. With paradichlorobenzene he found $W_1/W_2=0.3$. Pissanetsky[3] also studied relaxation in this compound.

Kawamori and Itoh[4] used steady-state methods to study Cl^{35} relaxation in $NaClO_3$ with the crystal at various orientations in the magnetic field. They found their data were best fitted with $W_1=10.8$ sec^{-1} and $W_2=1.56$ sec^{-1}, giving $W_1/W_2=6.9$. Ultrasonic excitation was used by Silver[5] to estimate $W_1/W_2\approx 1$ for I^{127} in KI. Recently, Daniel and Moulton[6] used pulse methods to study I^{127} relaxation in SnI_4. They found W_1/W_2 increased with temperature in the range 4–77 °K from about 0.1 to 0.2.

Several theories of quadrupolar relaxation have been given.[7] The expressions of Woessner and Gutowsky[7] appear to be giving order of magnitude agreement with experiment. This is discussed in detail in Sec. IVA below.

* Work supported by the National Science Foundation.
† Present address: Department of Physics, Kent State University, Kent, Ohio.
[1] R. V. Pound, Phys. Rev. **79**, 685 (1950).
[2] M. J. Weber, J. Phys. Chem. Solids **17**, 267 (1961).
[3] S. Pissanetsky, J. Chem. Phys. **42**, 675 (1965).
[4] A. Kawamori and J. Itoh, J. Phys. Soc. Japan **18**, 1614 (1963).
[5] A. H. Silver, J. Phys. Chem. Solids **23**, 273 (1962).
[6] A. C. Daniel and W. G. Moulton, J. Chem. Phys. **41**, 1833 (1964).
[7] D. E. Woessner and H. S. Gutowsky, J. Chem. Phys. **39**, 440 (1963).

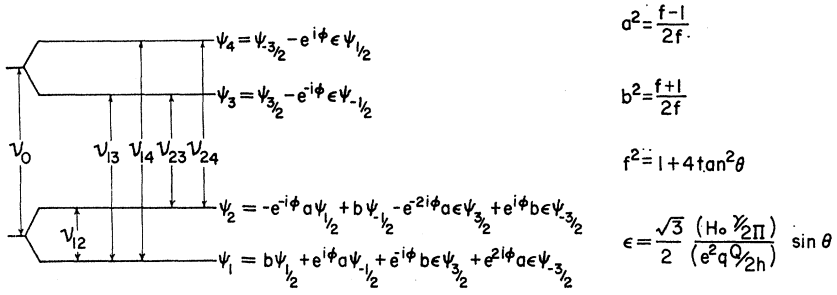

FIG. 1. Energy levels and eigenfunctions of a spin-$\frac{3}{2}$ nuclear quadrupole interaction perturbed by a magnetic field H_0 with orientation (θ,ϕ) relative to the axis of the electric-field gradient q. In $NaBrO_3$ the field gradient has axial symmetry so ϕ is arbitrary. In the present work $\nu_0=178.81$ Mc/sec, $H_0=7086$ G, $\theta\approx35°16'$, $a^2=0.212$, $b^2=0.788$, $\epsilon=0.021$. The frequencies of the five Zeeman transitions are given in Table I.

B. Summary

We have studied the system Br^{79} in a single crystal of $NaBrO_3$ in a magnetic field of 7086 G at room temperature. The energy levels, transitions, and eigenfunctions are shown in Fig. 1. In the absence of a magnetic field a single absorption at frequency ν_0 near 178.814 Mc/sec at room temperature is observed. The magnetic field H_0 has the orientation (θ,ϕ) relative to the direction of the principal electric-field gradient q of the crystal. All of the data have been taken with $\theta\simeq35°16'=\sin^{-1}1/\sqrt{3}$. The four higher frequencies, in the range 164 to 194 Mc/sec, will be designated pump frequencies; the lowest frequency is 10.7 Mc/sec.

The first observation[8] was that when rf energy at frequencies within the linewidths of the ν_{24} or ν_{23} transitions was applied to the crystal, the absorption intensity of the ν_{12} transition was increased by a factor of up to 4, depending on the power level of the pump oscillator. When the crystal was irradiated within the ν_{13} or ν_{14} transition widths, the 10.7-Mc/sec resonance intensity was reduced or showed net emission.

We decided to study these effects in detail with the hope of obtaining information on W_1 and W_2.

It appeared that the observations could be explained in terms of the difference of the spin populations of levels 1 and 2. Steady-state solutions of the rate equations were obtained and the data were extrapolated to give four maximum enhancements for the four pump frequencies in the limit of completely saturating pump power. Certain ratios of the maximum enhancements were expected to give a value for W_1/W_2. However, inconsistent values were obtained.

In general the maximum enhancements seemed too small, and it was thought that not all spins contributing to the unenhanced ν_{12} absorption were being reached by the pumping fields. An unusual relation here is that the frequency ν_{12} is independent of the magnitude of the field gradient q at the nuclear site, but depends on θ, the angle between H_0 and the axis of q. The frequencies of the transitions that were pumped are strongly dependent on both q and θ. Thus the observed small enhancements might be due to some of the sites having good enough θ for the spins on these sites to show absorption at ν_{12}, but having sufficiently defective q to shift ν_{ij} outside the pump frequency range. It is well known that point defects and strains or dislocations can change electric-field gradients. Several workers[9–12] have observed that defects reduce the intensity of nuclear-magnetic-resonance absorptions and explained their results in terms of quadrupole interactions.

We decided to give special attention to the *change* of the ν_{12} transition intensity due to the spin pumping, since only spins reached by the pump can contribute to this. This approach was successful and enabled us to obtain the value $W_1/W_2=5.3\pm2$. Using this value it was then inferred that only about 50% of the spins which should have been reached by the pump were in fact reached, explaining the difficulty with the enhancement measurements. Moreover, using the fact that $d\nu/d\theta$ is different for different pump transitions, some details of the data can be explained in terms of a distribution $g(\theta)$ of directions of q. This has been the most interesting, and perhaps the most important, part of this work.

II. THEORY

A. Frequencies and Eigenfunctions

The expressions for the frequencies of the five transitions involved in this work were obtained from a perturbation[13] calculation through second order in the quantity $\nu_M/\nu_0=2\gamma H_0h/e^2qQ$ (=0.042 here):

$$\nu_{13,24}=\nu_0\pm[(1+3\sin^2\theta)^{1/2}-3\cos\theta]\nu_M/2+3\sin^2\theta\nu_M^2/2\nu_0, \quad (1a)$$

$$\nu_{14,23}=\nu_0\pm[(1+3\sin^2\theta)^{1/2}+3\cos\theta]\nu_M/2+3\sin^2\theta\nu_M^2/2\nu_0, \quad (1b)$$

$$\nu_{12}=(1+3\sin^2\theta)^{1/2}\nu_M, \quad (1c)$$

$$\nu_0=e^2qQ/2h, \quad \nu_M=\gamma H_0/2\pi.$$

[8] J. W. Doane and R. A. Hultsch, Phys. Rev. **133**, A1085 (1964). [Eq. (1) is incorrect.]

[9] N. Bloembergen, *Report of the Conference on Defects in Crystalline Solids* (The Physical Society, London, 1955).

[10] M. H. Cohen and F. Reif, in *Solid State Physics*, edited by F. Seitz and D. Turnbull (Academic Press Inc., New York, 1957), Vol. 5.

[11] C. D. Watkins and R. V. Pound, Phys. Rev. **89**, 658 (1953).

[12] J. F. Hon and P. J. Bray, J. Appl. Phys. **30**, 1425 (1959).

[13] Y. Ting, E. R. Manring, and D. Williams, Phys. Rev. **96**, 408 (1954).

TABLE I. Frequencies of the transitions, slopes and intercepts of the lines of Fig. 4, induced transition probability coefficients f_{ij}, and (peak height)/area ratios of the curves of event 2.

ij	ν_{ij}[a] (Mc/sec)	Slope (arbitrary units)	Intercept $a_{ij}{}^{m}{}_{\max}$ (arbitrary units)	(Peak height)/area[b] (arbitrary units)	f_{ij}[c]
13	175.059	-0.62 ± 0.05	-1.85 ± 0.1	2.13 ± 0.08	0.768
14	193.572	-1.42 ± 0.12	-3.95 ± 0.2	1.84 ± 0.11	0.192
23	164.364	-1.10 ± 0.10	$+3.40\pm0.1$	1.82 ± 0.10	0.232
24	182.892	-0.55 ± 0.05	$+1.88\pm0.1$	2.16 ± 0.13	0.808
12	10.689	...	...	...	...

[a] Not all measured at the same temperature but at about 24.5°C. The values varied about ±30 kc/sec because of daily temperature variations.
[b] Averages with rms deviations from the lower pump-power half of the data for which the event-2 curves were not broadened.
[c] See text following Eq. (4).

The frequencies ν_0 and ν_M are the pure quadrupole frequency (for spin $\frac{3}{2}$) when there is no magnetic field, and the magnetic frequency if there were no quadrupole interaction, respectively. In this work $\nu_0=178.814$ Mc/sec and $\nu_M=7.559$ Mc/sec. The measured values of the pump frequencies are given in Table I. Equations (1) with $\theta=35°12'$ give the frequency values in Table I within 10 kc/sec.

The transitions and other terms are labeled with the numbers of the associated pair of levels. This is more elaborate than simply numbering the five transitions, but the explicit indication of the levels is useful. The asymmetry parameter η is negligibly small[13] so ϕ does not appear in the frequency expressions. Note that ν_{12} is independent of q. This is true even when the third-order perturbation term is included, for $\theta=35°16'$.

The eigenfunctions shown in Fig. 1 are complete through first order in ϵ ($=0.021$ here, one-half of the perturbation parameter above for $\theta=35°16'$). They are needed to calculate the transition probabilities per second given below. The angle ϕ was retained in the eigenfunctions as a check on the transition probability calculations. Since the field-gradient asymmetry is negligible, ϕ should not appear in the transition probabilities after terms containing ϵ higher then first order are discarded.

B. Thermal Transition Probabilities

The quadrupolar transition probabilities per second W_1 and W_2 are defined with the following time-dependent terms of the Hamiltonian[2]:

$$\mathcal{H}_{\pm1}=eQ(I_\pm I_z+I_z I_\pm)(V_{xz}\mp iV_{yz})/12, \quad (2a)$$

$$\mathcal{H}_{\pm2}=eQ(I_\pm{}^2)(V_{xx}-V_{yy}\mp 2iV_{xy})/24. \quad (2b)$$

The $V(t)$ are components of the field-gradient tensor and depend on time because the lattice is vibrating. The characteristic vibration frequency is about 10^{12} sec^{-1} and the vibration spectrum contains practically no components at the magnetic resonance frequencies. Spin-lattice relaxation is thus presumed to involve a Raman interaction of the spins with the phonons.[14] W_1 and W_2 are calculated from the spectral densities of the $V(t)$ as discussed by Das and Hahn.[15] For our purposes only the spin operators of Eq. (2) are needed with the eigenfunctions of Fig. 1 to obtain the following thermal transition probabilities $P_{ij}\propto\langle i|\mathcal{H}_{\pm1}+\mathcal{H}_{\pm2}|j\rangle^2$:

$$P_{13}=P_{24}=b^2W_1+a^2W_2, \quad (3a)$$

$$P_{14}=P_{23}=a^2W_1+b^2W_2. \quad (3b)$$

These expressions were given by Weber.[2] Cross terms in the squared matrix elements vanish under the assumption that there are no correlations between the different fluctuating $V(t)$ over a time of the order of T_1. Terms including ϵ^2 are discarded since $\epsilon^2\ll a^2, b^2$. Values of these parameters for this work are $\epsilon=0.021$, $a^2=0.212$, and $b^2=0.788$. P_{12} is considered negligible because it includes only terms with ϵ^2. A magnetic relaxation term $\mathcal{H}_{\pm1}{}^M$ has been neglected in these calculations, since the crystals were reasonably free of paramagnetic impurities.

C. Induced-Transition Probabilities

The transition probability per second induced by the pump oscillator at frequency ν_{ij} is designated A_{ij}. This is calculated using $A_{ij}=KH_1{}^2\langle i|I_++I_-|j\rangle^2$. The constant K includes terms which do not vary throughout the experiment and are the same for all pump frequencies; H_1 is the pump rf magnetic field. Using the eigenfunctions of Fig. 1, we obtain

$$A_{13}=KH_1{}^2(b^2-4ab\epsilon/\sqrt{3}), \quad (4a)$$

$$A_{14}=KH_1{}^2(a^2-4ab\epsilon/\sqrt{3}), \quad (4b)$$

$$A_{23}=KH_1{}^2(a^2+4ab\epsilon/\sqrt{3}), \quad (4c)$$

$$A_{24}=KH_1{}^2(b^2+4ab\epsilon/\sqrt{3}). \quad (4d)$$

It is convenient to express Eqs. (4) in the form $A_{ij}=KH_1{}^2f_{ij}$. Experimentally we obtain an induced rf voltage which is divided by ν_{ij} for a relative measure V of H_1. The quantity V^2f_{ij} is then a relative measure of A_{ij}. Values of f_{ij} are given in Table I.

[14] J. van Kranendonk, Physica **20**, 781 (1954).
[15] T. P. Das and E. L. Hahn, in *Solid State Physics*, edited by F. Seitz and D. Turnbull (Academic Press Inc., New York, 1958), Suppl. 1.

In the earlier part of this work zeroth-order eigenfunctions were used to calculate P_{ij} and A_{ij}. This amounts to neglecting terms containing ϵ, which gives $A_{13}=A_{24}$ and $A_{14}=A_{23}$ for the same H_1. The data are much better fitted by the rate equation solutions below when the ϵ terms are included in the A_{ij}.

The probability A_{12} due to the 10.7-Mc/sec spectrometer is included in the rate equations, but this term was kept negligible by operating the spectrometer at low level.

D. Rate Equations

The rf magnetic fields H_1 were always much less than the resonance linewidths, so spin-precession coherence effects were not considered. The data are adequately explained with solutions of the linear first-order rate equations for the spin populations n_i:

$$dn_i/dt=\sum_j[(P_{ji}+A_{ji})n_j-(P_{ij}+A_{ij})n_i] \qquad i,j=1,2,3,4;\ i\neq j. \quad (5)$$

The relation $A_{ij}=A_{ji}$, and the high-temperature approximation $P_{ji}=P_{ij}(1+h\nu_{ij}/kT)$ were used. Since Σn_i is constant, there are three independent equations whose steady-state ($dn_i/dt=0$) solutions were conveniently found using determinants. Similar equations are used to discuss four-level masers,[16] but the solutions there are generally more complicated than here because electronic spin-lattice relaxation probabilities are not so simply related to each other as are the P_{ij} in the present problem. [Eq. (3).]

The quantity observed was the absorption intensity of the ν_{12} transition so we write the solutions for n_1-n_2 when irradiating pump transition ij:

$$(n_1-n_2)_{ij}=(r_{ij}+s_{ij}A_{ij})/(t_{ij}+u_{ij}A_{ij}), \quad (6a)$$

$$r_{ij}=-8(hN/4kT)\nu_{12}(P_{ij}+P_{kj})P_{ij}P_{kj}, \quad (6b)$$

$$s_{ij}=-4(hN/4kT)P_{kj}[(2P_{ij}+P_{kj})\nu_{12}+(-1)^i(P_{ij}+P_{kj})\nu_{ij}], \quad (6c)$$

$$t_{ij}=-8(P_{ij}+P_{kj})P_{ij}P_{kj}-4(P_{ij}+P_{kj})^2(P_{12}+A_{12}), \quad (6d)$$

$$u_{ij}=-4(2P_{ij}+P_{kj})P_{kj}-4(P_{ij}+P_{kj})(P_{12}+A_{12}), \quad (6e)$$

$$i,k=1,2;\quad i\neq k;\quad j=3,4.$$

The approximation $P_{12}\nu_{12}\ll P_{ij}\nu_{ij}$ was used in obtaining r_{ij} and s_{ij}. The terms r_{ij} and t_{ij} are independent of ij since when there is no pumping ($A_{ij}=0$), the solution Eq. (6a) must be independent of ij. Also $u_{13}=u_{24}\neq u_{14}=u_{23}$ and $s_{13}=s_{24}\neq s_{14}=s_{23}$.

The most important experimental datum is the area under a curve, normalized to spectrometer sensitivity. This quantity is assumed to be proportional to the increase of n_1-n_2 above the thermal equilibrium value, due to the spin pumping. The expression for this increase when pumping at frequency ν_{ij} is

$$a_{ij}=(n_1-n_2)_{ij}-(n_1-n_2)_{A=0}. \quad (7)$$

The measured quantity, designated a_{ij}^m, has units of chart paper dimensions; a_{ij} has units of number of spins. Values of a_{ij} cannot be obtained from a_{ij}^m, because the absolute spectrometer sensitivity is not known.

Combining and rearranging Eqs. (6) and (7) gives the following linear relation of a_{ij} to a_{ij}/A_{ij}:

$$a_{ij}=-(t_{ij}/u_{ij})(a_{ij}/A_{ij})+(s_{ij}t_{ij}-r_{ij}u_{ij})/t_{ij}u_{ij}. \quad (8)$$

The data determine four such lines and from the ratios of their slopes, W_1/W_2 is determined by use of

$$\frac{(\text{slope})_{14,23}}{(\text{slope})_{24,13}}=\frac{f_{24,13}(b^2+a^2W_1/W_2)[1+a^2+(1+b^2)W_1/W_2]}{f_{14,23}(a^2+b^2W_1/W_2)[1+b^2+(1+a^2)W_1/W_2]}. \quad (9)$$

Equation (9) is obtained from the slopes in Eq. (8) with the u_{ij} of Eq. (6) and the assumptions $P_{12}, A_{12}\ll W_1, W_2$. The ratios $(\text{slope})_{14}f_{14}/(\text{slope})_{23}f_{23}$ and $(\text{slope})_{24}f_{24}/(\text{slope})_{13}f_{13}$ are independent of W_1 and W_2 and provide a check on the consistency of the slopes. The data were plotted as a_{ij}^m versus a_{ij}^m/V^2, i.e., using V^2 as a measure of A_{ij}. We could have used V^2f_{ij} for A_{ij} and then the f_{ij} would not appear in the slope ratio equations.

The ratios of the $a_{ij\,\max}$ are related to W_1/W_2 by

$$\frac{a_{ij\,\max}}{a_{kl\,\max}}=\frac{(st-ru)_{ij}u_{kl}}{(st-ru)_{kl}u_{ij}}. \quad (10)$$

The a_{ij} and A_{ij} are also related by the following expression obtained from Eq. (8):

$$a_{ij}/a_{ij\,\max}=A_{ij}/(A_{ij}+t_{ij}/u_{ij}). \quad (11)$$

This expression shows the approach to complete saturation of a pump transition for large A_{ij}.

The enhancement E_{ij} is defined by

$$E_{ij}=\frac{(n_1-n_2)_{ij}}{(n_1-n_2)_{A=0}}=1+\frac{a_{ij}}{(n_1-n_2)_{A=0}}. \quad (12)$$

The maximum enhancements for $A_{ij}\gg W_1, W_2$ are given by

$$E_{24,13\,\max}-1=\pm\frac{1+W_1/W_2}{1+a^2+(1+b^2)W_1/W_2}\frac{\nu_{24,13}}{\nu_{12}}, \quad (13a)$$

$$E_{14,23\,\max}-1=\mp\frac{1+W_1/W_2}{1+b^2+(1+a^2)W_1/W_2}\frac{\nu_{14,23}}{\nu_{12}}. \quad (13b)$$

[16] W. J. C. Grant, J. Phys. Chem. Solids **25**, 751 (1964).

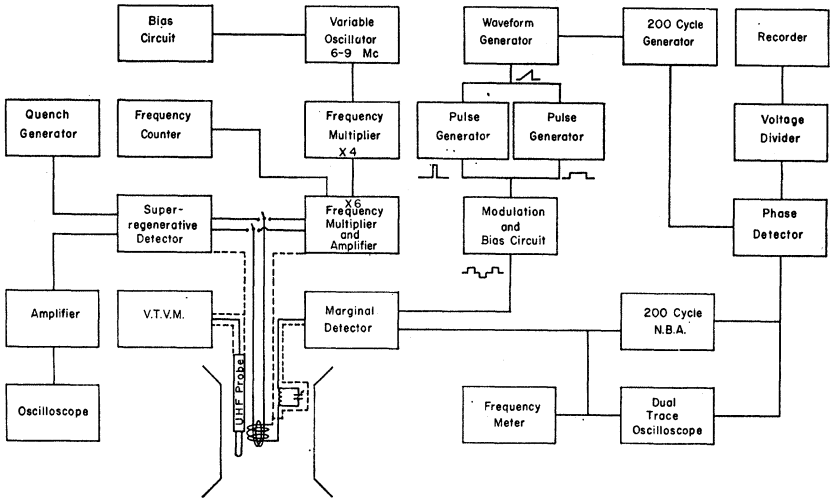

FIG. 2. Block diagram of the apparatus.

III. EXPERIMENTAL DETAILS

A. Spectrometers and Pump Oscillator

A block diagram of the apparatus is shown in Fig. 2. The circuits will be discussed in the order of their use in a typical run.

The first step was to orient the crystal which was mounted on and rotated about a horizontal axis whose gear system was fixed in the laboratory. The magnet rotated about a vertical axis. The high-frequency absorption at ν_{13} was observed by oscilloscope display of signals from a Lecher line super-regenerative spectrometer.[17] The crystal has four equivalent field-gradient directions and two of these were oriented with the same θ, near 35°16′, by overlapping the display of their ν_{13} signals. This was done to increase the ν_{12} absorption intensity. This particular choice of angle enabled us to orient both rf coils for optimum induced transition probabilities. Data can be taken at other angles, although at $\theta=0$ transitions ν_{23} and ν_{14} have zero-transition probability. Misorientation showed up as a broadening or splitting of the low-frequency absorption recording. It was necessary to reorient the crystal about once every hour while taking data, probably because the daily temperature rise caused the magnetic field direction to change by a few hundredths of a degree. The linewidth of the ν_{12} absorption, 2.5 kc/sec, corresponds to a 0.02° shift of θ, since $d\nu_{12}/d\theta=131$ kc/sec deg at $\theta=35°16'$.

The high-frequency spectrometer and the pump oscillator used the same rf coil around the crystal. After the crystal was oriented the spectrometer cathode lines were disconnected, and the plate lines including the vertical pair reaching down into the magnet gap were connected to the output of an rf power amplifier.[18] This was the pump-power source. It was driven with a signal originating at a variable frequency 6–9-Mc/sec oscillator which was multiplied by 24 to the range of the pump frequencies. The 6–9 Mc/sec oscillator frequency was varied with a Hughes 1N950 voltage variable capacitor in the tank circuit. The pump frequency was measured before the final frequency multiplication (X3) with a Computer Measurements Corporation 707B counter. The counter tuning eye was useful in retuning the multipliers when changing to a different pump frequency.

The pump power was varied by changing the $B+$ voltage on the Amperex 6252 tube of the final stage of the rf power amplifier. A relative measure of the magnetic field H_1 of the pump was obtained with a pickup loop coaxial with the pump coil. The induced signal was rectified with a 1N34 diode and measured with a vacuum-tube voltmeter (VTVM). The pickup system was not resonant over the range of pump frequencies. The power amplifier output stage was not resonant at any second harmonic of a pump frequency. To correct for nonlinearity of the diode, 0.04 V was added to the VTVM readings, which varied from about 0.4 to 3.5 V. These corrected readings were divided by the pump frequency to compensate for the frequency dependence of the induced voltage. The resulting values are designated V and assumed to be proportional to H_1 as discussed following Eqs. (4).

The low-frequency spectrometer used to detect the 10.7 Mc/sec absorption was similar to the marginal oscillator described by Hopkins.[19] This was operated at low enough levels that its induced-transition probabilities A_{12} were negligible compared to the thermal probabilities. This was checked by measuring the enhancements with different spectrometer levels at constant pump power. The enhancements were independent of spectrometer level at low levels but increased at higher levels, mainly because the unenhanced absorption was decreased.

[17] H. A. Dehmelt and H. Kruger, Z. Physik **130**, 356 (1951).
[18] *The Radio Amateur's Handbook* (American Radio Relay League, 1960), 37th ed., p. 443.
[19] N. J. Hopkins, Rev. Sci. Instr. **20**, 401 (1949).

In the earlier work[8] sine-wave magnetic modulation was used. This was undesirable because all the energy levels were modulated and the pump effects were somewhat smeared, and because it was possible to confuse absorption derivative change with intensity change. The bidirectional square-wave frequency-modulation technique of Verdieck and Cornwell[20] was adopted. In this, a square wave of alternating polarity is applied to a 1N950 voltage variable capacitor in the tank circuit of the low-frequency spectrometer, which results in the same wave form frequency modulation of amplitude ± 20 kc/sec of the 10.7-Mc/sec oscillations. The oscillator frequency is thus periodically shifted away from or to the ν_{12} resonance so that the line shape, not the derivative, is recorded. With alternating polarity the amplitude modulation, giving an unwanted signal, has Fourier components at odd multiples of half the frequency (200 cps) at which the resonance information is carried. In practice one distorts the square-wave symmetry slightly to empirically remove the 200-cps amplitude-modulation component. The signals from the marginal oscillator were amplified by the 200-cps narrow-band amplifier which blocked other unwanted signal components, were phase-detected, and displayed on a 10-mV-full-scale recording potentiometer. In cases of large enhancement the signals were precisely divided before recording. The system following the marginal oscillator was checked with dummy signals and found to be sufficiently linear over the range of the data.

The crystals were grown from aqueous solution of Fisher Scientific Company Reagent Grade $NaBrO_3$. The sample used for all the data presented here had a volume of about 2 cm^3. It was wrapped with a layer of plastic tape to reduce nonuniformity of the inductive heating described below, and the low-frequency coil was wound directly over the tape. The crystal and this coil rotated inside the high-frequency coil, about 3 turns of diameter 1.5 in. and length 1 in. The low-frequency coil, about 15 turns, was wound with its axis perpendicular to the two crystal-field gradient directions used. The axes of the rf coils were perpendicular to each other and to the direction of H_0.

B. Data

A typical chart record is shown in Fig. 3. The low-frequency absorption was always recorded first with the pump tuned away from any resonance. Frequency sweep was obtained with a motor-driven mechanical capacitor; this could have been accomplished with a voltage-variable capacitor. However, one cannot frequency modulate and sweep with the same 1N950 capacitor because shifting its operating point distorts the square-wave modulation and gives large base-line drift. The base-line drift shown in Fig. 3(a) is probably due to such an operating point change as the mechanical capacitor is varied. The trace shown represents a sweep over about 20 kc/sec; the width of the absorption is 2.5 kc/sec.

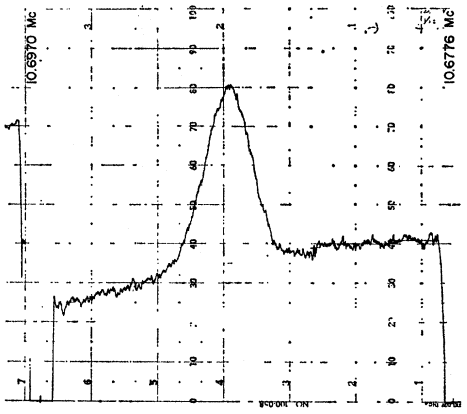

(a) Low Frequency Swept Through ν_{12}
High Frequency Off ν_{13}

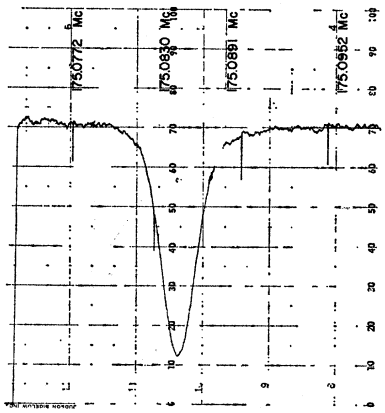

(b) High Frequency Swept Through ν_{13}
Low Frequency at 10.6880 Mc

FIG. 3 (a). Recording of the ν_{12} absorption with the pump oscillator tuned away from any resonance. The peak height is the only datum from this curve. This is referred to as event 1. (b). Recording when the low-frequency spectrometer is set at the center frequency of event 1 and the pump oscillator is swept over the line shape of ν_{13}. The area, peak height, and half-width are measured from this curve, which is referred to as event 2. The center frequency is greater than the value in Table I because this curve was taken at a few degrees lower temperature than the listed value.

After recording the ν_{12} absorption the low-frequency spectrometer was set on the center frequency, about 10.689 Mc/sec, of this resonance. This gives a signal which is the base line for the trace of Fig. 3(b). In this trace the low frequency was constant within random fluctuations of about ± 50 cps and the pump oscillator frequency was swept completely over the line shape of one of the high-frequency transitions. The resulting signal represents an increase or decrease of the *peak* absorption of the low-frequency resonance. In Fig. 3(b) the transition pumped is ν_{13} which makes $n_1 - n_2$ smaller or negative. Sweeping over ν_{24} or ν_{23} would give a signal with the opposite deflection. We do not

[20] J. F. Verdieck and C. D. Cornwell, Rev. Sci. Instr. 32, 1383 (1961).

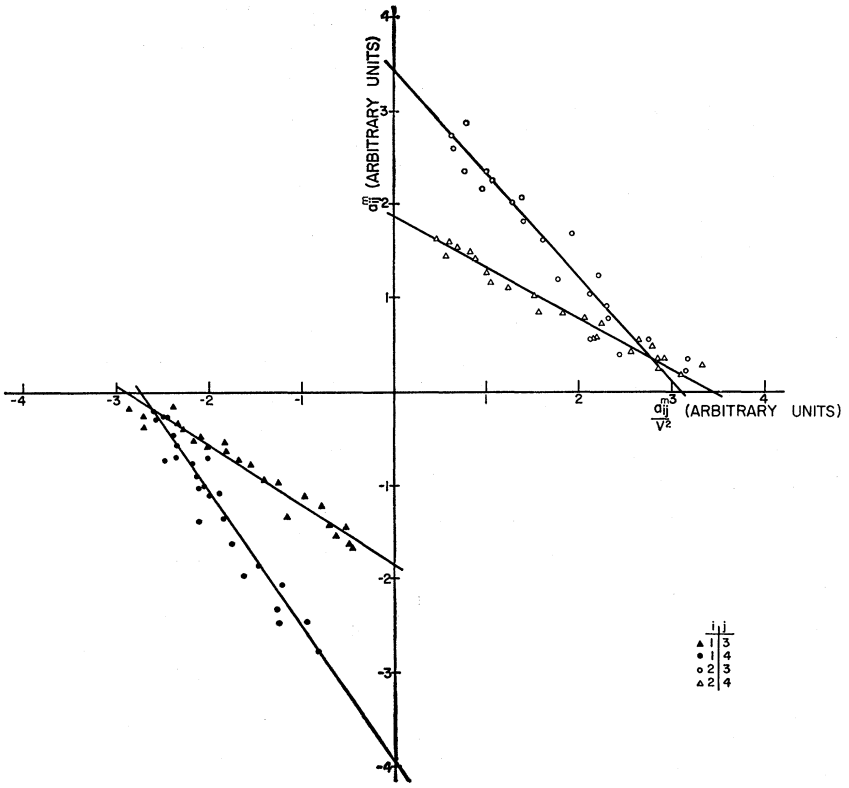

FIG. 4. Data plotted to be fitted by straight lines according to Eq. (8). a_{ij}^m are the areas under the event-2 curves divided by the peak heights of the event-1 curves (Fig. 3). The a_{ij}^m are proportional to the change of n_1-n_2, and are negative when pumping spins out of level 1. The slopes of these lines, drawn by inspection, are used with Eq. (9) to determine W_1/W_2.

regard the shape of the curve in Fig. 3(b) as simply an indirect recording of the ν_{13} absorption line shape. This is discussed in Sec. IVC. The recording of the ν_{12} absorption will be referred to as event 1, and the recording when sweeping the pump as event 2.

Four measurements were made on each pair of events: (1) The area in arbitrary planimeter units under the curve of event 2, considered negative when the absorption was decreased, and corrected for variations of the pump-frequency sweep rate; (2) the peak height h_2 of the event-2 curve in arbitrary units; (3) the width at half-maximum amplitude of the event-2 curve in frequency units; (4) the peak height h_1 of the event-1 curve in arbitrary units. The area (1) was divided by the peak height (4) to compensate for varying spectrometer sensitivity. The values of (4) scattered about $\pm 10\%$ during all runs. This ratio is designated a_{ij}^m and it is assumed to be proportional to a_{ij} in Eq. (7).

With each pair of recordings a relative measure V of the pump rf field H_1 was obtained. About 25 recordings with different pump levels were obtained for each of the four high frequencies.

All data were taken with the sample in air at room temperature, about 24°C. The crystal temperature rose 1–3°C when the higher pump powers were used. This was manifested in a shift of the center frequency of the curves of event 2, and a broadening of these curves because of temperature gradients in the crystal. We concluded that the pump rf field was inductively heating the low-frequency coil wound on the crystal. The consistency of the results indicates that the measured area under curve 2 was not significantly changed by the broadening. The temperature coefficient of the frequency of the high-frequency Zeeman lines is 17 kc/sec deg and the event 2 center frequency shifted as much as 60 kc/sec during the runs with the same pump frequency. The low-frequency transition, being independent of q, was not shifted by the heating.

Although the area measurement (1) was presumed to be reliable at all pump powers, the peak height (2) and width (3) measurements on the broadened curves were discarded. Important peak-height and width data were taken from about half the runs. The shapes of the event 1 and 2 curves have not been analyzed in detail. The (peak height)/area ratio and the width of the unbroadened event 2 curves were remarkably constant as the area increased by a factor of 5 and this was important in interpreting the data.

IV. RESULTS

A. a_{ij}^m versus a_{ij}^m/V^2: Slopes

The data are shown in Fig. 4. The straight lines are fitted by inspection. The values of the slopes, intercepts, and other quantities are given in Table I.

Equation (8) predicts

$$(\text{slope})_{14}f_{14}/(\text{slope})_{23}f_{23}=(\text{slope})_{13}f_{13}/(\text{slope})_{24}f_{24}=1.$$

TABLE II. Experimental values of W_1/W_2 from ratios of slopes of lines in Fig. 4 and using Eq. (9). The uncertainties are obtained by considering extreme slopes.

ij/kl	W_1/W_2
14/24	$4.0^{+3.8}_{-1.8}$
14/13	$5.2^{+2.1}_{-1.7}$
23/24	$5.2^{+6.5}_{-2.4}$
23/13	$6.8^{+3.8}_{-2.3}$
Weighted average $=5.3\pm2$	

The values in Table I give 1.07 ± 0.11 and 1.07 ± 0.12, respectively, for these ratios.

Equation (9) with the f_{ij} of Table I was plotted as slope ratios versus W_1/W_2. The experimental slope ratios were then compared to these curves to get the values of W_1/W_2 given in Table II. Our weighted average of these values is 5.3 ± 2.

For comparison with theory we follow the calculation of Woessner and Gutowsky.[7] Their theory is a recalculation of the Bayer[21] theory which dispenses with some of Bayer's assumptions. This theory is based upon molecular torsional oscillations as indicated by Raman spectra. Nuclear spin transitions are induced when these torsional motions are interrupted by other lattice vibrations with the result of fluctuations of the phases and amplitudes of the torsional oscillations.

The expressions developed by Woessner and Gutowsky are

$$W_1=(3/2)(\hbar\omega_Q^2/I\omega_\tau^3)(1/\tau_a)\coth(x/2), \quad (14)$$

$$W_2=(3/64)(\hbar\omega_Q/I\omega_\tau)^2[\tau_a/\sinh^4(x/2)] \quad (15)$$

and using an alternate calculation,

$$W_2=(3/16)(\hbar\omega_Q/I\omega_\tau)^2[\tau_a/(1-e^{-x})\sinh^2(x/2)], \quad (16)$$

where $\hbar\omega_Q=e^2qQ/2$, ω_τ is the torsional frequency, I is the moment of inertia for the molecular oscillation, $x=\hbar\omega_\tau/kT$, and τ_a is the average torsional level lifetime. To make a comparison of Woessner and Gutowsky's expressions and our experimental observations, it is necessary to have the values of the three parameters I, ω_τ, and τ_a. For the first two parameters we make use of the temperature dependence of the $NaBrO_3$ coupling constant obtained by Tipsword and Moulton.[22] They assumed two equivalent modes of oscillation for the BrO_3 group in $NaBrO_3$ and followed the Bayer-Kushida[23] theory to obtain values for the moment of inertia of the BrO_3 group and its torsional frequency. There are no independent measurements for the average torsional-level lifetime τ_a. This value is obtained from the expression $1/T_1=2(W_1+W_2)$ and a known value of T_1 at a particular temperature. We have made use of Hashi's[24] value of 2.1 msec for T_1 at room temperature.

[21] H. Bayer, Z. Physik **130**, 227 (1951).
[22] R. F. Tipsword and W. G. Moulton, J. Chem. Phys. **39**, 2730 (1963).
[23] T. Kushida, J. Sci. Hiroshima Univ. **A19**, 327 (1955).
[24] T. Hashi, J. Phys. Soc. Japan **13**, 911 (1958).

If the moments of inertia for both modes are taken to be 195 $(10)^{-40}$ gcm^2 and a torsional frequency of 108 cm^{-1} is assumed, then Woessner and Gutowsky's expressions can be used to obtain a value for τ_a. When this is done a situation is encountered similar to that found by Woessner and Gutowsky. Use of Eqs. (14) and (15) yields imaginary values for τ_a, whereas Eqs. (14) and (16) give real values for τ_a of 0.42 $(10)^{-12}$ sec and 7.6 $(10)^{-12}$ sec. The larger value gives W_1/W_2 much less than 1; the smaller value gives $W_1/W_2=18\pm4$. This uncertainty was calculated from the uncertainty in the T_1 value. Although the agreement with our measured value of W_1/W_2 does not appear to be good, one should expect only order of magnitude agreement in view of the uncertainty in the values of I and ω_τ. Not unreasonable adjustments of these parameters does give good agreement. The theory of Chang[25] seems to give poor agreement with our results.

B. $a_{ij}{}^m$ versus $a_{ij}{}^m/V^2$: Intercepts

The values of $a_{ij}{}^m{}_{\max}$ in Table I did not give consistent values for W_1/W_2 using Eq. (10). In trying to understand this it was useful to consider the data in terms of enhancements E_{ij} rather than population difference changes a_{ij}. The advantage here is that *maximum* enhancements can be calculated if one has a value of W_1/W_2. The $a_{ij\,\max}$ can also be calculated but these are only proportional to and not directly comparable with the $a_{ij}{}^m{}_{\max}$, since the spectrometer sensitivity is unknown.

The maximum enhancements $E_{ij\,\max}$ were calculated using Eqs. (13) and $W_1/W_2=5.3$. The $E_{ij}{}^m{}_{\max}$ were obtained from the experimental $a_{ij}{}^m{}_{\max}$ using the following expression:

$$E_{ij}{}^m{}_{\max}-1=\left(\frac{h_2}{h_1}\right)_{ij\,\max}=\left[\frac{\text{area}_2}{h_1}\right]_{ij\,\max}\left[\frac{h_2}{\text{area}_2}\right]_{ij}. \quad (17)$$

The subscripts in Eq. (17) refer to the curves of events 1 and 2; h is the peak height. The first bracket is $a_{ij}{}^m{}_{\max}$ as discussed in Sec. IIIB; values of the ratio in the second bracket are given in Table I. Values of $a_{ij}{}^m{}_{\max}$ in Table I were used with Eq. (17) to get the

TABLE III. Values of C_{ij} determined with Eq. (18) and half-widths of event 2 curves.

ij	$E_{ij\,\max}-1$ [Calc. from Eqs. (13)]	$E_{ij}{}^m{}_{\max}-1$ [From Eq. (17)]	C_{ij}	Half-width[a] (kc/sec)
13	−9.65	−3.94±0.2	0.41±0.02	2.74±0.07
14	−13.9	−7.27	0.52	3.23±0.11
23	11.8	6.19	0.52	3.18±0.12
24	9.93	4.06	0.41	2.63±0.11

[a] Averages with rms deviation from the lower-pump-power half of the data for which the event-2 curves were not broadened.

[25] C. E. Chang (unpublished).

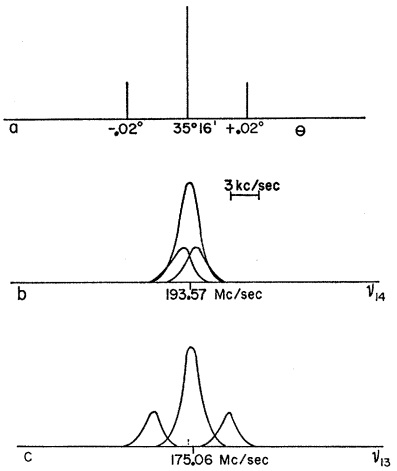

FIG. 5(a). A hypothetical discrete distribution of crystalline electric-field gradient directions. (b). Absorption spectrum of ν_{14} transitions of the hypothetical distribution, assuming perfect values of q and with dipolar broadening added. The frequency shifts of the defective site spins are ± 1 kc/sec, calculated using $d\nu_{14}/d\theta = -48$ kc/sec deg. The dipolar width is about 2.5 kc/sec. (c). Absorption spectrum of ν_{13} transitions. Frequency shifts are ± 3.6 kc/sec, calculated using $d\nu_{13}/d\theta = +180$ kc/sec deg. The curves in (b) and (c) represent direct absorption shapes at the respective frequencies, and not event-2 curve shapes.

$E_{ij}{}^{m}{}_{\max}$ in Table III. The $E_{ij}{}^{m}$ could have been obtained by measuring only peak heights without measuring the event 2 areas. The advantage of measuring areas was that this permitted data from broadened curves to be used and allowed us to include measurements at higher pump powers and make more precise extrapolations to the $a_{ij}{}^{m}{}_{\max}$.

The quantity $E_{ij}{}^{m}-1$ is a dimensionless measure of the peak height of the event 2 curve and was assumed to be proportional to the fraction C_{ij} of the spins contributing to the ν_{12} absorption which were reached by the pump at the center of the pump transition. The C_{ij} were calculated from

$$C_{ij} = (E_{ij}{}^{m}{}_{\max}-1)/(E_{ij\,\max}-1) \qquad (18)$$

and the values are given in Table III. Also shown in Table III are the average half-widths of the unbroadened event 2 curves. It is especially interesting that there appear to be only two different values of C_{ij} which are associated with only two different half-width values for the four pump frequencies.

The C_{ij} values are interpreted to mean that only 41% and 52% of the spins contributing to the ν_{12} absorption peak were reached by the pump fields H_1. The values of C_{ij} are not sensitive to the value of W_1/W_2 used to calculate $E_{ij\,\max}-1$. Values of W_1/W_2 within 5.3 ± 2 would give almost the same C_{ij}.

This interpretation is based on the idea that a spin site is characterized by its q and θ values, and that because of crystal imperfections the sites are distributed over ranges of these quantities. The distribution is centered on $\theta = 35°16'$ and the perfect crystal value of q. In particular we assume the existence of sites with perfect or nearly perfect values of θ but with defective values of q.

Perhaps the most interesting aspect of the transitions in this work is that ν_{12} depends on θ but is independent of q, whereas the pump frequencies ν_{ij} depend on both θ and q. To contribute to event 1 signal a spin must be on a site with θ within about $\pm 0.05°$ of $35°16'$ (actually the value of θ very near to this at which the data were taken). This signal is the ν_{12} absorption centered on 10.689 Mc/sec with half-width 2.5 kc/sec. A site with θ defective by 0.05° would have its ν_{12} center frequency shifted three linewidths from the observed center frequency above.

If the $a_{ij}{}^{m}{}_{\max}$ in Table I were larger the values of W_1/W_2 from Eq. (10) would be consistent with the results of Sec. IVA. Therefore it appeared that the event-2 intensities were too small, or that not all spins contributing to the peak of event 1 were being pumped. We believe that the spins with the relatively narrow distribution in θ of $35°16' \pm 0.05°$ have a sufficiently wide distribution in q so that about 50%, or $1-C_{ij}$, of them have a ν_{ij} value outside the frequency range over which the pump was swept. Why there are two different C_{ij} values is discussed in the next section.

C. Linewidth Observations

The width at half-maximum of the curves of event 2 was independent of pump power at the lower powers which did not produce observable crystal heating. However, the widths were dependent on which frequency was pumped. These widths with rms deviations are given in Table III. The explanations of the width differences and C_{ij} differences are based on the same idea. This is that the distribution of field-gradient direction $g(\theta)$ affects the event-2 curves differently because the $d\nu_{ij}/d\theta$ are different. The values of these are $d\nu_{13,24}/d\theta = \pm 180$ kc/sec deg, $d\nu_{23,14}/d\theta = \pm 48$ kc/sec deg, and $d\nu_{12}/d\theta = 131$ kc/sec deg.

It is important to keep in mind exactly what was directly observed in this work, viz., the change of the *peak* absorption of the low-frequency transition. The peak absorption is proportional to n_1-n_2 of spins whose value of ν_{12} is the same as the peak frequency. Such spins need not have perfect θ because their ν_{12} will vary over about 2.5 kc/sec, the low-frequency transition width, due to variations of the local dipolar magnetic field.

As the pump frequency is swept the first spins reached are those with a defective value of ν_{ij}, i.e., those with defective θ and/or q. Pumping of these does not directly give enhancement of the center of the low-frequency line. However, by spin diffusion to the center of the line shape being pumped, the center frequency of ν_{ij} is pumped indirectly and this shows up as event-2 signal.

In Fig. 5(a) is shown a hypothetical discrete dis-

tribution $g(\theta)$ of field gradient directions. This distribution consists of the perfect direction 35°16′ and two defective directions differing from perfect by 0.02° = 1.2′. For this illustration the spins of this distribution may all have the same q. Figs. 5(b) and c show the contributions to the ν_{14} and ν_{13} transitions of spins at sites with these directions, calculated using the $d\nu_{ij}/d\theta$, with dipolar broadening added. These figures may suggest at first that sweeping the pump over ν_{13} would give a wider event-2 curve than sweeping over ν_{14}, but this is opposite the experimental observations. The event-2 curve is not simply a record of the line shape of the ν_{ij} transition.

We think that pumping one of the defect angle transitions in Fig. 5(c) would not give much indirect enhancement because of the small overlap with the perfect angle transition line shape. But by cross relaxation through the overlapping lines of Fig. 5(b) the center frequency of ν_{14} may be indirectly pumped before the pump is swept to within the center-frequency line shape. Therefore, enhancement of the center of the low-frequency transition can occur over a wider range of pump frequency sweep, giving a broader event 2 curve for ν_{14} and ν_{23} as observed. There may also be indirect enhancement by cross relaxation through the line shape of the low-frequency transition.

The explanation of the C_{ij} differences follows the same ideas. C_{ij} is a measure of the effectiveness of the pump at the *center* of the ν_{ij} transition. The smaller C_{ij}'s are associated with transitions 24 and 13 with larger $d\nu_{ij}/d\theta$. Spins on sites with defective θ have their $\nu_{24,13}$ shifted more than $\nu_{14,23}$. Therefore there are fewer absorbing spins with frequencies near the center of $\nu_{24,13}$ and direct pumping is less effective with these transitions.

We have considered whether the differences in $d\nu_{ij}/dH_0$ can account for the C_{ij} and width differences. The values of these derivatives for this work are $d\nu_{13,24}/dH_0 = \mp 0.5$ kc/sec G, $d\nu_{14,23}/dH_0 = \pm 2.0$ kc/sec G, and $d\nu_{12}/dH_0 = 1.5$ kc/sec G. We were concerned about this point because H_0 varied about 0.5 G over the crystal volume. The pole caps had been selected for large air gap and high-field strength with sacrifice of homogeneity. For these reasons, not considering quadrupole effects, the ordinary absorption widths ν_{14} and ν_{23} may have been greater than the widths of ν_{13} and ν_{24}. Such broadening would influence the event-2 width and peak height, and might provide an alternative explanation of the event-2 widths being different. But it seems that inhomogeneity broadening would decrease the peak intensity of the high-frequency absorptions and produce decreased peak enhancements. The observations are contrary to this. For example, ν_{14} and ν_{23}, which would be more broadened by variation of H_0, give larger C_{ij} and hence larger peak enhancements. Consequently we think the $d\nu_{ij}/dH_0$ are not responsible for the observed effects. The high-frequency absorptions should have been recorded to compare linewidths and check these ideas, but we did not have regenerative spectrometer operation at these frequencies.

The dependence of signal intensity on defects indicated in this work may be compared with the results of Watkins and Pound.[11] They used a special calibration circuit to determine absolute spectrometer sensitivity, and found that the Br^{79} absorption in KBr had only 40% of the expected intensity. Quadrupole interactions due to defects spread part of this spectrum over such a wide frequency range that 60% of the intensity was not detected above the noise level. Defective θ or q values could have been responsible for such broadening.

Hon and Bray[12] observed an unusual crystal-orientation-dependent intensity of I^{129} in NaI and KI. They found that when a single-crystal [1,0,0] direction was nearly parallel to the laboratory magnetic field, the integrated intensity increased by a factor of three. The [1,0,0] direction was believed to be the axis of a screw dislocation, a much more ordered defect than usually affects magnetic resonance intensities. When H_0 was nearly in the [1,0,0] direction the distribution of defective field-gradient directions θ was much sharper than at other crystal orientations.

The present observations are more like those of Hon and Bray than of Watkins and Pound in that we find effects due to a distribution of θ values without knowing what fraction of all crystal spins contribute to the observed intensity. We have not measured the percent of spins contributing to the low-frequency absorption, but have observed that different fractions of these respond to different pump frequencies.

D. $a_{ij}{}^m/a_{ij}{}^m{}_{\max}$ versus V^2f_{ij}

Figure 6 shows the same data as in Fig. 4 plotted to be fitted by Eq. (11). The absolute values of A_{ij} are not known; the curves are fitted to the data at $a_{ij}{}^m/a_{ij}{}^m{}_{\max} = 0.5$. The quantity V^2f_{ij} was used for A_{ij}, rather than simply V^2 as in Fig. 4, so that the data would be fitted by two curves instead of four. The ratio t_{ij}/u_{ij} in Eq. (11) has only two values for a particular W_1/W_2, since t_{ij} is independent of ij and $u_{13} = u_{24} \neq u_{14} = u_{23}$, so there are only two different curves if V^2f_{ij} is the abscissa variable. If the ϵ terms are not included in calculating the f_{ij} in Eq. (4), the data in Fig. 6 are not fitted by only two curves. Thus the ϵ terms are significant in the induced-transition probabilities.

Figure 6 indicates what the C_{ij} and linewidth data in Table III show. This is that the pump frequencies are related in pairs 13,24 and 14,23. This plot is also interesting physically in that it shows the approach to complete saturation of the pump transitions. The maximum pump power used was about the same for all four transitions. However, for a given H_1 the 14 and 23 induced-transition probabilities were 3–4 times smaller than the 13 and 24 probabilities because of the differences in the eigenfunctions (different f_{ij}'s, Table I).

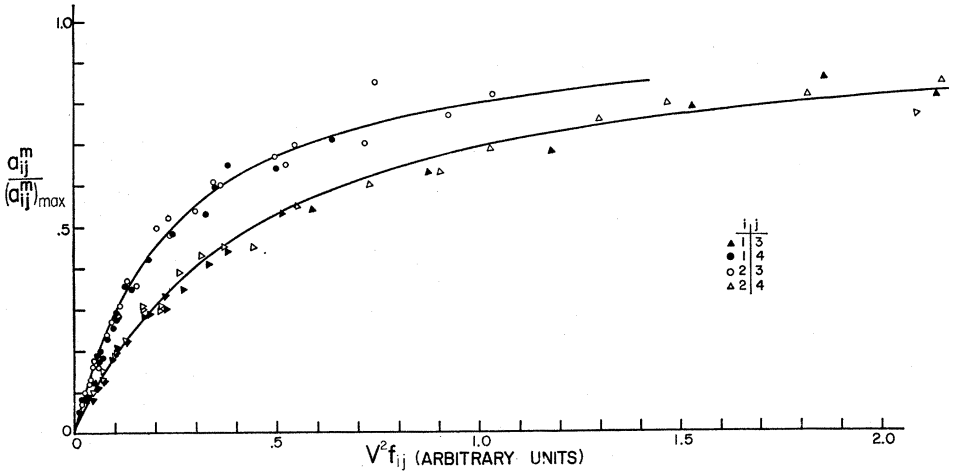

FIG. 6. The same data as in Fig. 4 plotted to be fitted by curves of the form of Eq. (11). The quantity V^2f_{ij} is used for A_{ij}, rather than simply V^2 as in Fig. 4, so that the data can be fitted by two curves instead of four. See Sec. IVD. Three points with V^2f_{ij} greater than 2.5 and which are fitted by the lower curve are not plotted. The maximum pump fields H_1 were about the same for all frequencies, but the f_{ij} factors result in different transition probabilities.

E. Miscellaneous Observations

Several experiments were performed early in this work with a poorer crystal than used for the data above. This crystal had a volume of about 1 in.^{3}, was grown faster, and had visible occlusions and cracks. It gave a low-frequency absorption line about 10% wider than did the crystal finally used. One experiment was to set the low-frequency spectrometer at various frequencies within the ν_{12} transition line shape, not only at the center, and observe the event-2 signal. This curve had the same shape in all cases, in particular was not asymmetric, but diminished in amplitude as the spectrometer was set further from the ν_{12} center. The frequency of the pump oscillator at the peak of the event-2 curve shifted in one direction as the spectrometer frequency was moved from the ν_{12} center.

Another experiment was to set the pump frequency within the ν_{ij} width and sweep the spectrometer completely through the low-frequency transition. With the pump at the center frequency of ν_{23}, not all the ν_{12} shape was enhanced as its width was about 10% less than the width of the unenhanced line. The center of ν_{12} was enhanced by a factor of about 4. When the pump was set about one-half linewidth from the center of the ν_{14} transition, the spectrometer trace showed part absorption and part emission.

A third experiment was to orient the crystal so two symmetry axes were at slightly different θ with ν_{12} center frequencies separated by one linewidth. This gave a symmetric double-peak absorption when unenhanced. When the pump was set on ν_{24} to pump one of the peaks, the trace was asymmetric with one peak much more enhanced than the other. It may be that cross-relaxation can be studied quantitatively, as well as qualitatively, by such experiments.

In an exploratory experiment we observed a weak free induction decay of the ν_{12} resonance following a $\pi/2$ pulse at 10 Mc/sec. The signal was only above the noise level when enhancing power was applied. Studies of transient effects are attractive as they may lead to understanding of the miscellaneous cross-relaxation effects.

Finally we note the observation by oscilloscope display of the enhanced and inverted ν_{12} transition. This was carried out during a demonstration of a Northern Scientific Company digital averaging instrument. This device observed the signals when the low-frequency spectrometer was frequency modulated with a 60 cps sine wave over five ν_{12} linewidths.

V. CONCLUSION

The nuclear spin-pumping phenomena which were studied here can be described with steady-state solutions of the rate equations and the assumption that crystal imperfections affect signal intensity. With some improvements in technique it should be possible to reduce the uncertainty in W_1/W_2. Possibly more interesting is to further test the notion that different $d\nu_{ij}/d\theta$ cause different intensities and widths. It will of course be desirable to compare relaxation and defect information from different compounds available as about 1-cm^3 single crystals, and from crystals with systematically introduced defects.

It may be possible to get information on the $g(\theta)$ distribution without using double irradiation, by studying the dependence on the magnetic field H_0 of the intensities of the Zeeman lines. This is because the $d\nu_{ij}/d\theta$ are proportional to H_0, so as H_0 is increased intensities should decrease.

Note added in proof. The expressions for ψ_3 and ψ_4 in

Fig. 1 are incorrect. The correct expressions are $\psi_3=\psi_{3/2}-e^{i\phi}\epsilon\psi_{1/2}$ and $\psi_4=\psi_{-3/2}-e^{-i\phi}\epsilon\psi_{-1/2}$. S. L. Segel and R. G. Barnes [Phys. Rev. Letters **15**, 886 (1965)] have observed the $\nu_{12}=2\nu_M$ transition for $\theta=90°$ in several polycrystalline samples including sodium bromate. It should be possible to enhance or invert this signal by pumping, although special attention must be given to the direction of the pump H_1 for $\theta=90°$ to ensure nonzero induced transition probabilities. However, we do not expect to obtain W_1/W_2 by spin-pumping a polycrystalline sample because for $\theta=90°$ the P_{ij} for the pump transitions differ only by small terms proportional to ϵ.

ACKNOWLEDGMENTS

We wish to thank M. M. Hulse for electronic services and O. Roloff for machine work and assistance in the assembly of the apparatus.

PHYSICAL REVIEW VOLUME 143, NUMBER 1 MARCH 1966

Electron-Gas Spin Susceptibility*

D. R. HAMANN†
Department of Electrical Engineering, Massachusetts Institute of Technology, Cambridge, Massachusetts
AND
A. W. OVERHAUSER
Scientific Laboratory, Ford Motor Company, Dearborn, Michigan
(Received 23 September 1965)

The wave-vector-dependent spin susceptibility of an electron gas is calculated taking dynamically screened electron interactions into account. A quasiparticle approach is developed to deal with the self-energy and screening effects of the electron correlations, and the energy and mass of a quasiparticle at the Fermi surface are calculated for a wide density range. The susceptibility is found using a linearized self-consistent-field treatment of the quasiparticles and numerical solution of the resulting integral equation. It does not show singular or anomalous behavior at large wave vector as in the Hartree-Fock approximation. The density dependence of the zero-wave-vector susceptibility is found to be in better agreement with experiment than that of previous calculations. Statically screened interactions are also used in a series of calculations, and it is shown that a long- but finite-range interaction can lead to anomalies in the susceptibility at large wave vectors.

1. INTRODUCTION

THE effect of the Coulomb interaction on the magnetic properties of the electrons in a simple metallic conduction band has received a good deal of attention recently. One of the authors has shown that it renders the paramagnetic plane-wave state of the free-electron-gas model unstable within the Hartree-Fock (HF) approximation, an antiferromagnetic spin-density wave (SDW) state having lower energy.[1] The long-range components of the Coulomb interaction are most important in creating this instability. Correlation corrections to the HF approximation for the paramagnetic electron gas have been studied extensively, and it is agreed that the long-range components of the Coulomb interaction make a major contribution to the correlation energy, especially at high densities.[2] Therefore it is apparent that correlation corrections should be applied to a calculation of the SDW instability. The evaluation of the energy of a SDW state with correlation is an extremely difficult undertaking, however, and our goal in this paper is more modest. By calculating the wave-vector-dependent spin susceptibility of the paramagnetic state and including correlations, the stability of this state under infinitesimal deformations can be investigated, and this is the calculation we shall discuss.

The wave-vector-dependent spin susceptibility is defined by the following thought experiment: A static magnetic field $\mathbf{H}(\mathbf{x})=H_0\boldsymbol{\varepsilon}\cos(\mathbf{Q}\cdot\mathbf{x})$ is applied to the electrons, and the spin magnetization is measured. For the free-electron gas and for small H_0, it has the same spatial dependence and polarization, $\mathbf{M}(\mathbf{x})=M_0\boldsymbol{\varepsilon}\cos(\mathbf{Q}\cdot\mathbf{x})$. The susceptibility is defined as $\chi(Q)=M_0/H_0$ in the limit as H_0 goes to zero. In the approximation we shall consider, neglecting field-orbit spin-orbit, and dipolar spin-spin couplings, χ does not depend on the angle between $\boldsymbol{\varepsilon}$ and $\mathbf{Q}$. The change in internal energy associated with the magnetization is proportional to $M_0^2/\chi(Q)$. Therefore, if the paramagnetic state is unstable, we should expect to calculate a nega-

* The portion of this research, which was performed at the Massachusetts Institute of Technology, was supported by the Office of Naval Research, Contract No. Nonr-1841(72).

† Now at Bell Telephone Laboratories, Murray Hill, New Jersey.

[1] A. W. Overhauser, Phys. Rev. **128**, 1437 (1962).

[2] For a review of much of this work, see D. Pines, *The Many Body Problem* (W. A. Benjamin, Inc., New York, 1961).